PostPINN-EM: Fast Post-Voiding Electromigration Analysis Using Two-Stage Physics-Informed Neural Networks

Subed Lamichhane[1], Wentian Jin[1], Liang Chen[1,2], Mohammadamir Kavousi[1] and Sheldon X.-D. Tan[1]

[1]Department of Electrical and Computer Engineering, University of California, Riverside, CA 92521

[2]School of Microelectronics, Shanghai University, Shanghai 201800

slami002@ucr.edu, wjin018@ucr.edu, cl5555cl@outlook.com, mkavo003@ucr.edu, stan@ece.ucr.edu

Abstract—In this paper, we propose a novel machine learning-based approach, called *PostPINN-EM*, for solving the partial differential equations for stress evolution in a confined metal interconnect multi-segment trees during the post-voiding stage for fast electromigration (EM) check for interconnects. The new approach is based on an enhanced two-stage Physics-Informed Neural Networks (PINN) framework in which the physics law for a single wire is enforced first and then atomic flux conservation and stress continuity at the inter-segment junctions of wire segments are then fulfilled to reduce the number of variables of loss functions for the fast training process. Existing two-stage PINN method uses supervised learning method for modeling a single wire under various atomic flux conditions for the first stage, which turns out to be much more difficult for post-voiding phase due to arbitrary non-zero initial conditions. To mitigate this problem, we propose a new closed-form parameterized formula for stress solution of single wires with variable boundary conditions based on the Laplace transformation methods. Furthermore, we derive the analytic solutions for wire segment with and without voiding as not all the wire segments will have voids during the post-voiding phase. Numerical results on some synthesized multi-segment interconnects show that the proposed *PostPINN-EM* can achieve more than 100X speedup compared to FEM based tool COMSOL with the expense of less than 1% accuracy. Compared to the state of the art tool EMspice v1.0 [1], this method can achieve more than 25X speedup with similar accuracy compared to golden results from COMSOL.

Index Terms—Electromigration (EM) postvoiding phase, physics-informed neural network (PINN), multisegment interconnect, hydrostatic stress assessment

I. INTRODUCTION

Electromigration (EM) remains a significant reliability concern for copper-based interconnects in current and future technology nodes as the current density increases and the interconnects' dimensions shrink. Therefore, it is critical to accurately assess aging and reliability of both interconnects and devices during the design process.

The well-accepted Black and Blech-based EM models [2], [3] have faced growing criticism for being overly conservative and only applicable to a single wire segment [4], [5]. To address these issues, several physics-based EM models and assessment techniques based on Korhonen's equations [6] have recently been proposed [7], [8], [9], [10], [11], [12], [13], [14], [15], [16], [17], [18], [1], [19], [20].

Recent studies have shown that accurate circuit-level analysis of EM stress requires tree-level modeling of wire segments in an interconnect tree [21]. To achieve this, the partial differential equation (PDE) of hydrostatic stress evaluation in multi-segment metal wires under blocking material boundary conditions, known as Korhonen's equation, must be solved. However, solving Korhonen's equation and other PDEs using traditional numerical methods remains a significant challenge due to their inherent limitations. Therefore, several physics-based EM models and assessment techniques based on Korhonen's equations have been proposed to address these limitations.

Recently, the so-called physics-informed neural networks (PINN) or physics-constrained neural networks (PCNN) have been proposed to learn and encode physics laws expressed by nonlinear partial differential equations (PDE) for complex physical, biological or engineering systems [22], [23]. In PINN method, the physics laws, boundary condition and initial conditions of the PDEs are explicitly enforced via loss functions in neural networks and have shown promising results for small PDE problems with a small number of variables. Another significant benefit of PINN/PCNN idea is that they are mesh-free compared to traditional FEM or FDM based methods.

PINN based approach has been applied to solve Korhonen's equation recently [24], [25], [26]. In [24], PINN has been used directly to solve for the stress evolution in the confined metal for simple straight interconnects. Jin *et al.* further developed a hierarchical PINN method in which two training stages are used to slow training and convergence issues of plain PINN [25]. In this method, the first stage DNN model for a single wire was built by supervised learning method. Recently Hou *et al.* proposed to use some analytic formula in the final loss functions of the PINN method [26]. However, all of those PINN approaches are for nucleation phase analysis. No analysis has been done for more complicated post-voiding phase with more complicated boundary conditions and initial non-zero stress conditions. *Actually our initial study shows that with non-zero initial conditions, it is very difficult, if not impossible, to train a DNN model with sufficient accuracy using the supervised learning method.*

In this work, we try to mitigate the mentioned problem and extend the two-stage PINN concept to solve the post-voiding phase of EM failure processes in multi-segment interconnects tree. Our new contributions in this work are as follows:

- First, we propose to apply two-stage PINN concept to solve PDE for the post-voiding phase of the stress evaluation on the confined multi-segment interconnect metal wires for the first time. Compared to the nucleation phase, one challenge we face is to build accurate parameterized

stress models for a single wire under various aomtic flux boundary conditions and arbitrary non-zero conditions for segment with and without voids.

- To mitigate the mentioned problem, instead of using the supervised learning as done in [25], we propose a closed analytic formula for single interconnect segment. This analytical solutions are obtained by solving Korhonen's equation using the Laplace transformation method. Our analytical solution takes initial stress into account. Furthermore, we derive analytical solutions for both voidless segments and segments with void by taking corresponding physics into consideration. The analytical solutions we use depend totally on the physical and material properties of the wires.
- For our second stage, we use PINN to enforce atomic flux conservation and stress continuity at the inter-segment junctions of wire segments based on the analytic solution of single segments from the first stage. As we only enforce the physics law at the a few inter-segment junctions, this can lead to dramatic reduction of variables in the loss functions and speedup of the training process.
- Experimental results on some synthesized multi-segment interconnects show that the proposed *PostPINN-EM* can achieve more than 100X speedup compared to FEM based tool COMSOL with the expense of less than 1% accuracy. Compared to the state of the art tool EMspice v1.0 [1], this method can achieve more than 25X speedup with similar accuracy compared to golden results from COMSOL.

The structure of this paper is as follows: Section II reviews the physics behind the problem we are solving. Section III reviews the existing tools that are being used to solve the EM stress evolution. In Section IV the structure and underlying principles of our proposed method is explained. Experimental results to support our claims are presented in Section V. Finally, section VI concludes this paper.

II. PROBLEM DEFINITION

Electromigration (EM) is a critical reliability issue in nanoscale Very Large Scale Integration (VLSI) circuits. To address this issue, researchers have been exploring physics-based numerical and analytical techniques, which are gaining popularity for EM stress assessment. In this section, we will discuss the physics behind the nucleation and post-voiding phase EM stress evolution in multisegment interconnect trees. By examining these processes, we hope to gain insights into how EM stress affects the reliability of VLSI circuits, and how it can be analyzed through effective design and simulation techniques.

In confined metal wires with high current density, atoms migrate from the cathode to the anode ends due to the momentum exchange between electrons and metal atoms [2]. This phenomenon is known as electromigration. As time goes on, this migration of metal atoms from the cathode to the anode can cause depletion of atoms at the cathode end and accumulation of atoms at the anode end. This depletion and accumulation can cause the formation of voids and hillocks in the confined metal wires, which can jeopardize the performance of the interconnect.

Many techniques have been proposed to assess the reliability of metal interconnects due to electromigration (EM). Blech's limit [3] and Black's MTTF equation [2] are the

two traditionally accepted methods for EM reliability analysis. These techniques provide an estimate of when the interconnects can fail. However, they are losing attention because Black's MTTF only works for a single line segment, and none of these tools can provide an estimate of hydrostatic stress evolution. Korhonen's equation [6] defines the physics of EM evolution in confined metal wires in terms of a set of partial differential equations (PDEs). Korhonen's equation can be expanded to solve for hydrostatic stress in multisegment interconnects [27], [18]. Equation (1) is the Korhonen equation for multisegment interconnect for the nucleation phase.

$$\frac{\partial \sigma_{ij}(x,t)}{\partial t} = \frac{\partial}{\partial x}\left[\kappa_{ij}\left(\frac{\partial \sigma_{ij}(x,t)}{\partial x} + G_{ij}\right)\right], t > 0$$

$$BC: \sigma_{ij_1}(x_i,t) = \sigma_{ij_2}(x_i,t), t > 0$$

$$BC: \sum_{ij}\kappa_{ij}\left(\frac{\partial \sigma_{ij}(x,t)}{\partial x}\bigg|_{x=x_r} + G_{ij}\right)\cdot n_r = 0, t > 0 \quad (1)$$

$$BC: \kappa_{ij}\left(\frac{\partial \sigma_{ij}(x,t)}{\partial x}\bigg|_{x=x_b} + G_{ij}\right) = 0, t > 0$$

$$IC: \sigma_{ij}(x,0) = \sigma_{ij,T}$$

Here, $\sigma_{ij}(x,t)$ is the stress on the interconnect segment ij connected to the nodes i and j. In (1), G_{ij} is the EM driving force at segment ij, which is given by $G_{ij} = \frac{e\rho J_{ij}Z^*}{\Omega}$ with J_{ij} being the current density on segment ij. The diffusivity of stress, κ_{ij}, is defined as $\kappa_{ij} = D_a B\Omega/(k_B T)$, where D_a is the effective atomic diffusion coefficient, B is the effective bulk elasticity modulus, k_B is the Boltzmann's constant, T is the absolute temperature, and E_a is the EM activation energy. e is the electron charge, ρ is the resistivity, Z^* is the effective charge. First BC in (1) states that the stress is continuous at the inter-segment junction boundaries i.e. at $x = x_r$. Second BC represents atomic flux conservation at the inter-segment junctions and the third BC is for blocking terminal boundaries $x = x_b$ where the atomic flux is zero. The inward unit normal direction of the interior junction node x_r on the branch ij is denoted by n_r. IC is the initial condition with states that the initial stress distribution at segment ij is given by $\sigma_{ij,T}$.

In multisegment interconnect trees, a void is nucleated at the cathode node where the steady-state nucleation stress exceeds the critical stress σ_{crit}. The time at which void is nucleated is the nucleation time t_{nuc}. For time $t > t_{nuc}$, the void continues to grow and the physics of stress evolution is no more similar to the nucleation phase. After the void is nucleated, the stress at the void surface sharply reduces to zero under a large stress gradient [28]. For the interconnect segment where the void is nucleated, the set of equations during the post-voiding phase is given by (2) [28]. This equation assumes $x = 0$ node to be the cathode node of the wire where the void is nucleated. For the case where void is nucleated at $x = L$, the BC's can be changed accordingly.

$$PDE: \frac{\partial \sigma(x,t)}{\partial t} = \frac{\partial}{\partial x}\left[\kappa\left(\frac{\partial \sigma(x,t)}{\partial x} + G\right)\right], t > 0$$

$$BC: \frac{\partial \sigma(0,t)}{\partial x} = \frac{\sigma(0,t)}{\delta}, x = 0, t > 0$$

$$BC: \frac{\partial \sigma(0,t)}{\partial x} = -G, x = L, t > 0 \quad (2)$$

$$IC: \sigma(x,0) = \sigma_{nuc}(x,t_{nuc}), t = 0$$

The equation presented assumes that the void interface has

an effective thickness δ, which is infinitely small compared to other lengths in the interconnect tree. The analysis of post-voiding stress is performed by counting time t from the nucleation time t_{nuc}, and the initial stress distribution for this phase is assumed to be the stress distribution at the time of void nucleation. This approach allows for the modeling of stress evolution in a single confined wire after void nucleation. For multisegment interconnect trees, there can be cases where multiple cathode nodes exceed the critical stress. In such case, a void is nucleated at the node with the maximum stress [29]. To solve multisegment interconnects in postvoiding phase, equation (2) can be used for the segment containing the void, while other voidless segments can be solved using equation (1) However, to obtain the stress solution for the entire interconnect tree, boundary conditions (BC) representing the continuity of stress and the conservation of atomic flux should be employed [29].

In this work, we propose a hierarchical solver for the postvoiding stress in interconnects using modern neural network-based techniques. In the first stage, we use a Laplace transform-based analytical solution to solve for single segments with or without void. In the second stage, stress continuity and flux conservation are enforced using a physics-informed neural network (PINN).

III. RELATED WORKS

A. Traditional numerical approaches for solving PDEs

Traditionally, conventional numerical and analytical methods are used to solve the PDEs represented by (1), and (2), to solve for EM stress in nucleation and post-voiding phase [28], [18], [16], [27], [1], [30], [19]. In spite of being satisfactorily accurate, these methods suffer from issues like computational complexity and scalability. For example, finite element based method [16] and finite difference method [30] can accurately solve for stress in complex multisegment structures. However, the method requires discretization of time and space which makes this method computationally costly. On the other hand, analytical method like [19] is computationally very fast but can only solve for straight line wires. The optimal trade-off between speed and computational complexity is hard to find using conventional numerical and analytical approaches.

B. Neural networks based approaches for solving PDEs

With the recent advancements in machine learning and deep neural networks (DNN), the realm of pattern recognition has witnessed a remarkable acceleration and simplification [31], [32]. DNNs excel in accurately mapping complex non-linear functions while offering substantial speed enhancements compared to conventional tools. This capacity of DNNs has found application in solving intricate partial differential equations (PDEs) related to physical problems [33], [34]. Recently Jin *et al.*[35] introduced a generative learning-based approach named *EM-GAN* to address transient EM stress, exhibiting promising gains in both speed and accuracy over traditional methods. However, this method, being image-based, falls short in adequately representing complex multisegment interconnects, limiting its applicability to a broader range of problems. In response, the *EMGraph* approach[36] was proposed, rectifying this limitation by introducing graphical representations of interconnects and employing graph neural networks to tackle EM stress.

While supervised neural network models like *EM-GAN* and *EMGraph* demonstrate effectiveness, their reliance on large training datasets poses a constraint. In contrast, unsupervised techniques like "physics-informed neural networks" (PINNs) [37], [23] or "physics-constrained neural networks" [38], [39] do not necessitate prior training datasets. PINNs utilize loss functions of DNNs to enforce the physical laws relevant to the given problem, providing a powerful means to address complex physical systems without the need for extensive training data.

However, only very simple PDE problems were demonstrated in [37], [40], [38], [41], [23] although some progress were made for more complicated aerodynamics simulations recently [42]. Recently, a PINN-based approach for EM analysis has been proposed [24]. The method tries to improve the PINN method to better handle the temperature-dependent diffusivities for metal atom migrations. It tries to add more neurons representing some pre-determined allocation points and time instances into the neural networks. This method slightly improves the plain PINN method by achieving better training accuracy at the cost of longer training time under the same number of neurons. Jin *et al* proposed a hierarchical approach *HeirPINN-EM* [25], which solves the nucleation phase EM problem more accurately than methods like *EMGraph*. Recently Hou *et al.* further proposed hybrid PINN methods to model the nucleation phase of EM failure process [26]. This method adds some additional constraints in terms of analytical formula of simplified solutions into the final loss functions to reduce some variables.

IV. NEW TWO-STAGE PINN SOLVER FOR POST-VOIDING PHASE

This section presents our solver for post-voiding phase EM stress analysis for multi-segment interconnect wires. We first present the overall flow of the proposed two-stage PINN solving algorithm. Then we explain each stage in detail.

A. The overall algorithm flow

The proposed two-stage PINN solving algorithm is shown in Fig 1. It consists of two stages, first stage is an analytical solution for single wires with parameterized boundary conditions as shown in the pink region. The second stage is the rest of the modules in this figure. It is basically a PINN based neural network framework where we use simple multilayer perceptron (MLP) network.

As shown in Fig 1, *PostPINN-EM* takes a multisegment interconnect tree as input. The MLP in the second stage takes the features corresponding to each junction as input and predicts $f^-(t)$ and $f^+(t)$ for the segments connected to the junctions taking care of flux conservation. These flux information are then passed to the first stage analytical solution. The analytical solution also gets the physical properties and initial stress distribution of each segment as shown in the figure. The first stage analytical solution uses these information to calculate the EM stress distribution on each segment. The calculated stress is used in the loss function, which enforces stress continuity at the inter-segment junctions. This loss function is used to optimize the prediction of $f^-(t)$ and $f^+(t)$ through back-propagation. After the MLP is trained, stress $\sigma(x,t)$ at a given position x and aging time t can be inferred using the framework.

B. First stage: physics-law enforcement via analytical solution for a single segment

In the first stage, we enforce the physics-law for stress evaluation within a single wire segment under different bound-
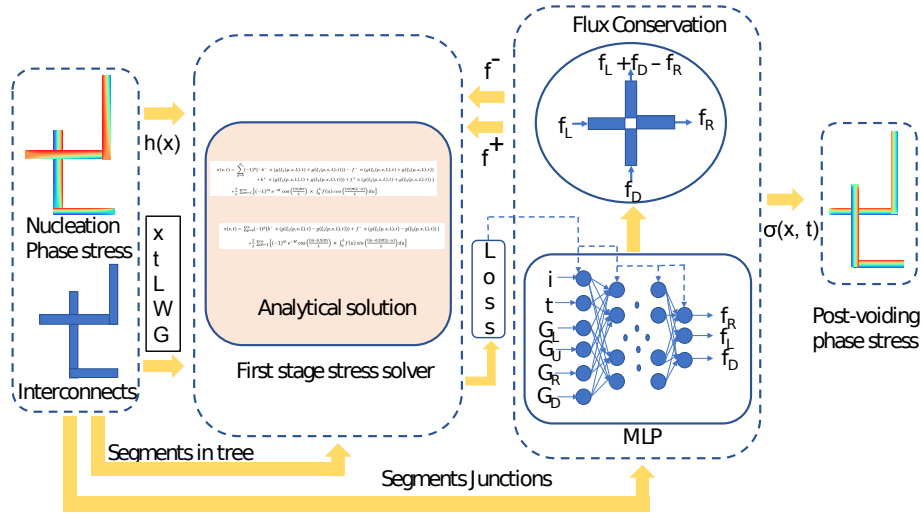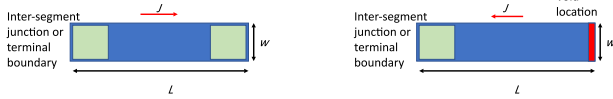
Fig. 1: *PostPINN-EM* framework.

ary conditions, atomic fluxes. This is achieved by solving Korhonen's equation for a single wire segment under those complicated boundaries and initial conditions analytically. Once we obtain this analytic solutions, then we can enforce the physics-laws (conserving atomic flux and stress continuity) at the inter-segment junctions in the second-stage PINN framework via the stochastic gradient descent method.

(a) A single segment without void.

(b) A single segment with void at $x = L$.

Fig. 2: Single interconnect segments that are part of a multi-segment interconnect tree in the postvoiding phase.

In a multi-segment interconnect tress at the postvoiding phase there can be one segment with void and multiple segments without void. Fig 2 illustrates the single segments with voids and voidless segments. We remark that in this work, we only assume on void in the whole multi-segment wire tree, which is the dominant case for EM failure [43]. For a single segment, we assume L to be its length, w to be its width and J be the static or effective current density on the segment. In our notation, a wire segment is defined from $x = 0$ to L, where $x = 0$ is the preceding node ('-' superscript) and $x = L$ is the consequent node ('+' superscript).

1) Analytical solution for a segment without void: We first consider the wire segment without void as a void can only nucleated in one segments in multi-segment tree. In this case, the boundary ends of the segment without void can be either an inter-segment junction or a terminal boundary as shown in Fig 2a. Our goal is to derive the analytical solution for these segments under variable atomic flux (stress gradients) boundary and initial conditions. In other words, the boundary condition becomes stress gradient variables. Specifically, we define stress gradient variables at the left/bottom node as $\phi^-(t)$ and at the right/top node as $\phi^+(t)$. As a result, the Korhonen's equation with adjustable (parametrized) boundary conditions for a wire segment without void can be written as

(3):

$$PDE : \frac{\partial \hat{\sigma}(x,t)}{\partial t} = \frac{\partial}{\partial x}\left[\kappa\left(\frac{\partial \hat{\sigma}(x,t)}{\partial x} + G\right)\right], t > 0, 0 < x < L$$

$$BC : \frac{\partial \hat{\sigma}(x,t)}{\partial x} = \phi^-(t), x = 0$$

$$BC : \frac{\partial \hat{\sigma}(x,t)}{\partial x} = \phi^+(t), x = L$$

$$IC : \hat{\sigma}(x,0) = \sigma_{nuc}(x, t_{nuc}) = h(x)$$

$$(3)$$

In Eq. (3), $\hat{\sigma}(x,t)$ denotes the new stress solution obtained from the new Korhonen's equation, $\phi^-(t)$ and $\phi^+(t)$ are adjustable boundary conditions equivalent to the spatial gradients of the stress at the boundaries. We assume $h(x)$ to be the initial stress distribution, which actually is the stress distribution at the nucleation time t_{nuc}. Turn out that (3) can be solved by the Laplace transformation method, which leads to the following analytic solution for $\sigma_i(\hat{x},t)$ in the time domain:

$$\hat{\sigma}(x,t) = \sum_{p=0}^{P}\{-\frac{d\phi^-(t)}{dt} * (g(\zeta_1(p,x,L),t) + g(\zeta_3(p,x,L),t))$$
$$- \phi^-(0)\,(g(\zeta_1(p,x,L),t) + g(\zeta_3(p,x,L),t))$$
$$+ \frac{d\phi^+}{dt} * (g(\zeta_2(p,x,L),t) + g(\zeta_4(p,x,L),t))$$
$$+ \phi^+(0)\,(g(\zeta_2(p,x,L),t) + g(\zeta_4(p,x,L),t))\}$$
$$+ \frac{2}{L}\sum_{m=1}^{M}(-1)^m\{e^{-M}\cos(m\pi x/L)$$
$$\times \int_0^L h(u)\cos\left(m\pi(L-u)/L\right)du\}$$

$$(4)$$

Here, p and m are positive integers such that $0 \leq p \leq P$ and $1 \leq m \leq M$. For the value of P, it is suggested in [44] to keep three dominant parts, i.e. $P = 2$. The value of M is determined experimentally and discussed in detail in the result section. In (4), the symbol $*$ represents the convolution operator defined by $a(t) * b(t) = \int_0^t a(\tau)b(t-$

$\tau)d\tau$. This convolution can be performed very fast using the Gauss-Legendre quadrature algorithm [26]. Functions $\zeta_1(p,x,L), \zeta_2(p,x,L), \zeta_3(p,x,L)$, and $\zeta_4(p,x,L)$ and $g(x,t)$ are defined as follows:

$$\zeta_1(p,x,L) = (2p+2)L - x, \ \zeta_2(p,x,L) = (2p+1)L - x,$$
$$\zeta_3(p,x,L) = (2p)L + x, \qquad \zeta_4(p,x,L) = (2p+1)L + x,$$
$$g(x,t) = 2\sqrt{\frac{kt}{\pi}}e^{-\frac{x^2}{4kt}} - x \times erfc\{\frac{x}{2\sqrt{kt}}\}$$

(5)

2) Analytical solution for a segment with a void: Now we consider the wire segment with a void. In this case, we assume that one end of the segment can be an inter-segment junction or a terminal boundary whereas another end is the void node. Fig 2b shows a single segment with a void at $x = L$ end. At $x = 0$, which can be either an inter-segment junction or a terminal boundary, an adjustable boundary condition in the voidless case is used. We rewrite the boundary condition at $x = L$ as $\hat{\sigma}(L,t) = 0$. For a very small value of δ in (2), BC used in the equation at the void location is similar to BC used here [45]. The boundary conditions for the segment with a void at the consequent node of a wire segment, i.e., at $x = L$, can be written as shown in (6).

$$BC : \frac{\partial\hat{\sigma}(x,t)}{\partial x} = \phi^-(t), \ x = 0$$
$$BC : \hat{\sigma}(x,t) = 0, \ x = L$$

(6)

Similar to the solution for the voidless segment, using the Laplace transform method, the solution for the single segment with a void at $x = L$ is obtained:

$$\hat{\sigma}(x,t) =$$
$$\sum_{p=0}^{P}(-1)^p\{\frac{d\phi^-(t)}{dt} * (g(\zeta_1(p,x,L),t) - g(\zeta_3(p,x,L),t))$$
$$+ \phi^-(0)\left(g(\zeta_1(p,x,L),t) - g(\zeta_3(p,x,L),t)\right)\}$$
$$+ \frac{2}{L}\sum_{m=1}^{M}(-1)^{m+1}\{e^{-M}\cos((m-0.5)\pi x/L)$$
$$\times \int_0^L h(u)\sin\left((m-0.5)\pi(L-u)/L\right) du\}$$

(7)

Similarly, for the condition where the void location is at the preceding (left/bottom) i.e at $x = 0$ location, the boundary condition is set to $\hat{\sigma}(x,t) = 0$ at $x = 0$ and $\frac{\partial\hat{\sigma}(x,t)}{\partial x} = \phi^+(t)$ at $x = L$. Following the similar Laplace transform method we can obtain the analytical solution for this case as well.

In (3) and (6), the integrals $\int_0^L h(u)\cos\left(m\pi(L-u)/L\right) du$ and $\int_0^L h(u)\sin\left((m-0.5)\pi(L-u)/L\right) du$ are calculated using the Gauss-Legendre quadrature algorithm for faster calculations. Equation (8) shows an example of how these integrals are calculated using the Gauss-Legendre quadrature algorithm.

$$\int_0^L h(u)\cos\left(m\pi(L-u)/L\right) du$$
$$= \frac{L}{2}\sum_{j=0}^{N_g} A_j h(u_j)\cos\left(m\pi(L-u_j)/L\right)$$

(8)

Here $u_j = x_j(\frac{L}{2}) + \frac{L}{2}$ and $\{A_j\}_{j=1}^{Ng}$ and $\{x_j\}_{j=1}^{Ng}$ are the Gaussian weights and zero points of Legendre polynomial. N_g is the number of discrete integration series. The accuracy

of the integral value and hence the stress depends on N_g [26]. In this work the best value for N_g for optimal accuracy and speed is determined experimentally and presented in the results section.

C. Second stage: PINN for stress continuity and flux conservation at inter-segment junctions

In the second stage of our method, we estimate the complex flux information at the inter-segment junctions of the multisegment interconnect tree via the PINN-based solving method. Basically, we design a DNN network so that its loss function is built in such a way that stress continuity and flux conservation are perfectly enforced at every boundary and inter-segment junctions throughout the whole interconnect tree as shown in Fig 1. Specifically, in *PostPINN-EM*, we use the stochastic gradient descent method based on simple multi-layer perceptron (MLP) networks to find the atomic flux information at those inter-segment junctions while enforcing atomic flux conservation and stress continuity. Fig 3 shows the
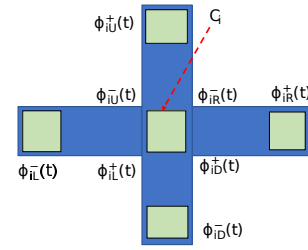

Fig. 3: General structure of the interconnects at the internal junction

typical cross structure of the interconnects connected together at the inter-segment junctions of a multisegment interconnect. In the figure, C_i is the ith inter-segment junction of the multisegment interconnect. Note that the number of segments that can be connected to the each node is less than or equal to 4. The segments connected to i^{th} junctions are differentiated using subscript $s = L, U, R, D$, for segments connected to the left, top, right, and bottom respectively. Here, $\phi_{is}^{-/+}(t)$ denote the stress gradients of the segments at the position s connected to junction i. The initial values for $\phi_{is}^{-/+}(t)$ can be calculated as [26]:

$$\phi_i^+(0) = \frac{w_R G_R + w_U G_U - w_L G_L - w_D G_D}{w_L + w_R + w_D + w_U},$$
$$when \ i \ is \ on \ s= L \ or \ s=D \ position$$
$$\phi_i^-(0) = \frac{w_L G_L + w_D G_D - w_R G_R - w_U G_U}{w_L + w_R + w_D + w_U},$$
$$when \ i \ is \ on \ s=R \ or \ s=U \ position$$

(9)

$$\phi_i^{+/-}(0) = -G_i,$$
$$at \ terminal \ boundary$$

Here, w_s represents the width and G_s is the driving force of segment s connected to node C_i. The input parameters to equations (4) and (7) are as follows: (a) physical parameters, i.e. L, w, which are determined from the given interconnect tree on a case by case basis, (b) initial stress, i.e. $h(x)$, which is extracted from the nucleation phase solution, (c) flux information at the boundaries, i.e. $\phi^-(0), \phi^+(0), \frac{d\phi^-(t)}{dt}$ and

$\frac{d\phi^+(t)}{dt}$. Eq (9) gives $\phi_i^-(0)/\phi_i^+(0)$. Thus, to get predictions for each wire segment, $f^-(t) = \frac{d\phi^-(t)}{dt}$ and $f^+(t) = \frac{d\phi^+(t)}{dt}$ are the only unknowns to be determined in the second stage.

As shown in Fig 1, our second stage PINN model uses an MLP model to estimate $f^-(t)$ and $f^+(t)$ for each segment using the features at the junctions where these segments are connected. The MLP takes i, t, G_L, G_U, G_R, G_D as input features. Here, i is the inter-segment junction label, t is aging time, G_L, G_U, G_R, G_D are driving forces corresponding to left, upper, right and, lower segment connected to the junction with label i. The output of the MLP are f_L, f_R, f_D which are atomic flux corresponding to the left, right, and lower segment respectively. Atomic flux conservation given by BC in (1) is enforced while calculating flux information f_U corresponding to the upper segment by following the transformation described in [25], [26]. Using f_L, f_R, f_D, and f_U at junctions, $f^-(t)$ and $f^+(t)$ are calculated for each segment and provided to the first stage analytical solution. The correctness of these predicted quantities is ensured through iterations of backpropagations based on the following physics-informed loss function:

$$L = \frac{1}{N_I \times K_i} \sum_{i=1}^{N_I} \sum_{k=2}^{K_i} (\hat{\sigma}_k(t) - \hat{\sigma}_{k-1}(t))^2 \quad (10)$$

where N_I denotes the number of inter-segment junctions in the interconnects, K_i represents the number of connected wires at i-th junction, which ranges between 2 and 4. $\hat{\sigma}_k(t)$ is the k-th predicted stress result for the current junction at aging time t. The loss function is the mean squared error (MSE) of all predicted stress at inter-segment junctions, which serves as a measurement of stress discontinuity at boundaries. Here, the loss function doesn't use any pre-calculated data. It is rather based on the physics behind stress continuity that is given by BC in (1).

V. NUMERICAL RESULTS AND DISCUSSIONS

This section presents the implementation details, accuracy, and performance evaluation of the proposed method, *PostPINN-EM*. The analytical solution and MLP model were both implemented in Python 3.8.12 with PyTorch 1.7.1. The training and testing were conducted on a Linux server with 2 Xeon E5-2699v4 2.2 GHz processors and an Nvidia Titan RTX GPU. To update the parameters of the MLP, we used Adam optimization with a learning rate of 10^{-3}. Xavier initialization was used to initialize the parameters of the MLP in the second stage. The MLP used in this work consisted of 5 hidden layers, and we found the optimal configuration of neurons to be $[6, 100, 100, 100, 100, 100, 3]$. For all Gauss-Legendre quadrature algorithm based integral calculation, $N_g = 8$ is used as a result of trade-off between calculation speed and accuracy. It is observed that as N_g increases the accuracy tends to increase and the calculation time tends to increase as well [26].

A. Data preparation and scaling

To obtain data related to the physical and material properties of the interconnect segments, we first read the given multisegment interconnect structure. We extract the physical properties of individual segment i, such as L_i, w_i, and G_i, assuming κ is the same for all segments. We sample the spatial points x between $[0, L]$ and use temporal points $t = 0$ to $1 \times 10^9 s$ with a step size of $1 \times 10^7 s$ for our study. For this work,

we assume that these interconnect structures have already been solved for the nucleation phase using other methods. We extract the initial stress information $h(x)$ and void location from the nucleation phase results.

The input parameters used by the analytical solutions and the MLP have vastly different magnitudes. Therefore, data scaling is necessary to regularize the parameters used by the MLP. In this work, we use k_x to scale x, k_t to scale t, and k_σ to scale $\sigma(x,t)$. Other parameters are scaled according to the following equation:

$$k_\sigma \sigma(x, t, \kappa, G) = \sigma_{sc}(x_{sc}, t_{sc}, \kappa_{sc}, G_{sc})$$
$$= \sigma_{sc}(k_x x, k_t t, \frac{k_x^2}{k_t}\kappa, \frac{k_\sigma}{k_x}G) \quad (11)$$

where $x_{sc}, t_{sc}, \kappa_{sc}, G_{sc}$, and σ_{sc} represent the scaled version of x, t, k, G, and σ. By performing scaling on the parameters x, t, κ, G, we can calculate the scaled stress σ_{sc}. We then restore this scaled stress to its original magnitude using k_σ. For this work, we have used $k_x = 1 \times 10^{-5}$, $k_t = 1 \times 10^{-7}$, and $k_\sigma = 1 \times 10^{-8}$.

B. Speed and accuracy of first stage analytical solver

The first-stage analytical solution provides accurate stress solution when precise stress gradients are provided for boundary conditions. To verify the accuracy of the first stage and assess its speed, we compared it against results from COMSOL under various predefined stress gradients. We randomly generated around 200 wire segments with lengths ranging from $10\mu m$ to $50\mu m$. Throughout this whole study we use interconnects with equal widths of $1\mu m$. These wire segments were assigned current densities ranging from $-5 \times 10^9 A/m^2$ to $5 \times 10^{10} A/m^2$. Other constants were set to $e = 1.6 \times 10^{-19}C$, $Z^* = 10$, $E_a = 1.1eV$, $B = 1 \times 10^{11}$, $D_0 = 5.2 \times 10^{-5}m^2/s$, $\rho = 2.2 \times 10^{-8}\Omega m$, $\Omega = 8.78 \times 10^{-30}m^3$, $\sigma_{crit} = 5 \times 10^8 Pa$.

For analysis of our first stage solver, the wire segments were assigned non-zero flux at the boundaries to model the segments in the multisegment trees. For each segment, we sampled 30 spatial position points $x \in [0, L]$ and used 100 temporal points ranging from 0 to 1×10^8 seconds for aging time t. We solved these individual segments using COMSOL and compared them against our analytical solution. We used the root mean square error (RMSE) as a metric for error, with the range of stress $\sigma(x,t)$ in this study found to be -1.1×10^8 to 4.6×10^8. Using our analytical solution, we observed an average RMSE of 3.3×10^4. This RMSE relates to an average error of 0.006%. To solve for a single segment, the average runtime of the analytical solution was observed to be 0.01 s, while the average runtime of the COMSOL program to generate the stress solution for a segment is around 7.5 s. The average runtime speedup of the analytical solution compared to COMSOL can be inferred to be around 750X. These results indicate that the first stage analytical solution is both very fast and accurate when compared to FEM-based COMSOL.

Fig 4 shows the comparison of our analytical solution against COMSOL for both voidless segments and segments with void. We obtained these results using $M = 5$ in the analytical solutions. The optimal value of $M = 5$ is determined experimentally and the same value is used throughout this work.
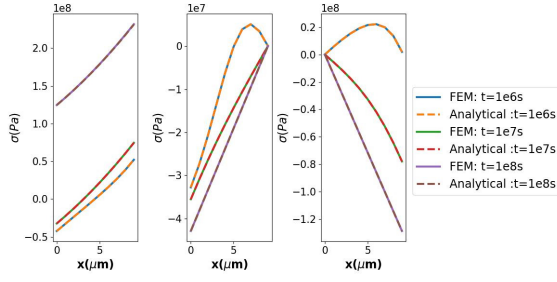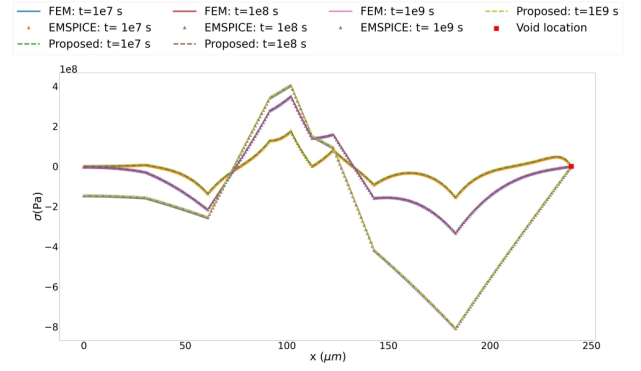
Fig. 4: Comparison of the solution obtained from analytical solution with the solution from FEM-based COMSOL for single interconnect segment.
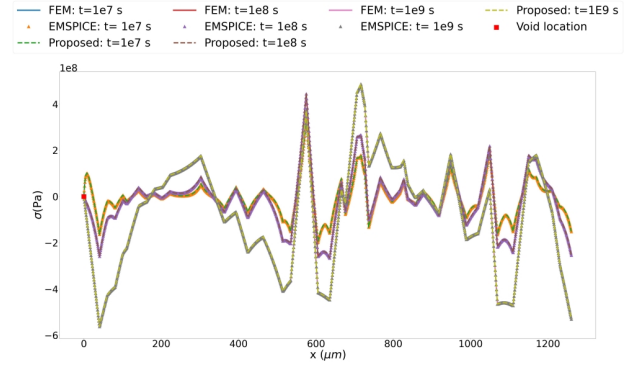
C. Speed, accuracy, and scalability of PostPINN-EM

Now we evaluate the accuracy, speed, and scalability of the whole *PostPINN-EM* method. To this end, we generated 500 multisegment interconnect lines. The multisegment interconnect lines consisted of a varying number of segments ranging from 5 to 250. For each segment, we sampled 30 spatial points from $x \in [0, L_i]$, where L_i is the length of the ith segment. We used 100 equally spaced temporal points ranging from 0 to 1×10^9 for aging time. We first solved these multisegment interconnect structures using COMSOL for the nucleation phase, and then extracted the initial stress and void location information from the stress distribution for our post-voiding phase analysis. It is important to note that we did not consider nucleation phase metrics when analyzing the accuracy and speed of our method, as our focus is solely on the postvoiding phase stress evolution.
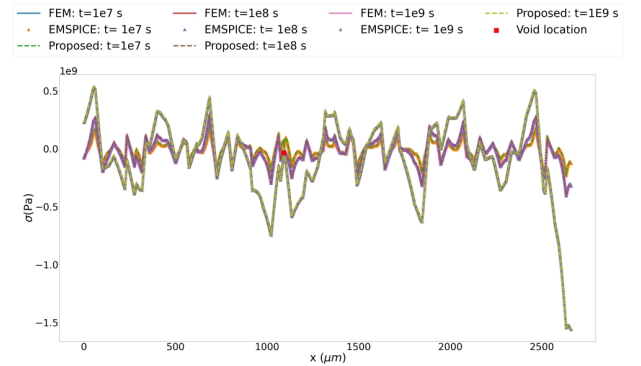
Analyzing solution of multisegment interconnect straight lines, we observed that the range of stress $\sigma(x,t)$ was within the range of $-7.2 \times 10^8 Pa$ to $5.6 \times 10^8 Pa$. The average RMSE error for the 500 multisegment interconnect lines was observed to be $2.5 \times 10^6 Pa$ compared to COMSOL which relates to an average error of 0.19%. To compare the performance of our proposed method, we also solved the multisegment interconnect structures using EMspice V1.0 (or EMspice) [1], which resulted in an average RMSE of $8.9 \times 10^5 Pa$ compared to COMSOL. The average error of EMSpice compared to COMSOL relates to 0.07 %. Fig 5 shows the $\sigma(x,t)$ distribution calculated using COMSOL, EMspice, and our proposed method at different values of the time. We observed that the solution obtained from our proposed method agrees very closely with COMSOL and EMspice even as the number of segments increased, demonstrating the scalability of our method. For the 500 multisegment straight interconnects, we observed an average training speed of around 20 seconds. Furthermore, the average inference speed of the proposed method is 0.86 seconds. On the other hand, COMSOL's average runtime to solve for the interconnects, based on meshed FEM methods, was noted to be around 1600 seconds. If we compare the average runtime of the COMSOL, and the total time (training+inference), the average speedup we see is around 76X. For EMSpice the average runtime is found to be 400 seconds. Hence compared to EMSpice, an average speedup of 20X is observed. Table I presents the comparison of the speed and performance of *PostPINN-EM* against EMspice and COMSOL on multisegment straight lines. We can observe from the table that as the number of segments increases, the sum of the training and inference time of the proposed method

(a) Ten-segment straight interconnect line.

(b) Fifty-segment straight interconnect line.

(c) Hundred-segment straight interconnect line.

Fig. 5: Comparison of results obtained from analytical solution with FEM-based COMSOL and state-of-the-art EMspice for multisegment straight interconnect lines.

becomes less than the runtime of EMspice and COMSOL. This is because the proposed method requires less discrete integration series compared to EMspice and COMSOL. In terms of accuracy, the error percentage for *PostPINN-EM* increases with the number of segments. The error percentage is calculated using the RMSE against COMSOL. The accuracy of the proposed method seems to follow the accuracy of EMspice very closely as can be seen in the table.

To demonstrate the effectiveness of *PostPINN-EM* on non-straight interconnect trees, we conducted experiments on an additional 500 multisegment interconnect trees. The number of segments for the trees ranged from 10 to 300 segments. These multisegment trees are solved for postvoiding phase stress using both COMSOL and our proposed method. The

TABLE I: Performance and accuracy comparisons with existing methods on multisegment straight lines

# of wires	COMSOL		EMspice		PostPINN-EM			
	Runtime (s)	Error (%)	Runtime (s)	Error (%)	Inference time(s)	Training time(s)	Speedup vs. COMSOL	Speedup vs. EMSpice
5	21.9	0.04	8.4	0.07	0.11	6.17	4.12X	1.37X
25	150.2	0.03	67.3	0.08	0.21	14.61	10.14X	4.54X
50	954.7	0.06	92.6	0.07	0.42	19.85	47.02X	4.56X
75	1556.4	0.07	120.2	0.11	0.63	22.63	66.79X	5.15X
100	1963.1	0.09	320.3	0.13	0.84	26.83	71.38X	11.64X
150	2535.3	0.12	596.3	0.21	1.31	32.54	75.1X	17.6X
200	3645.3	0.14	891.5	0.26	1.59	36.22	96.4X	23.57X
250	4325.8	0.23	1056.6	0.31	1.82	39.76	104.2X	25.46X

performance and accuracy analysis of our method on multisegment trees compared to COMSOL is presented in Table II. The results showed an average RMSE of $7.6 \times 10^6 Pa$ compared to COMSOL. The stress range for this case was found to be in $-9 \times 10^8 Pa$ to $4 \times 10^8 Pa$. This results in an average error of around 0.5%. Fig 6 illustrates the stress distribution

TABLE II: Performance and accuracy comparisons with existing methods on multisegment trees

# of wires	COMSOL	PostPINN-EM			
	Runtime (s)	Error (%)	Inference time(s)	Training time(s)	Speedup vs. COMSOL
27	181.52	0.31	0.24	15.91	11.2X
88	2136.7	0.52	0.76	24.72	83.8X
173	3235.9	0.85	1.47	35.54	87.4X
287	4668.4	1.06	1.91	48.61	96.7X

across different positions of the multisegment interconnect tree at various time intervals. The figure shows that the stress distribution obtained from our proposed method closely follows the result obtained from COMSOL for interconnect segments with varying numbers of segments at different times. For multisegment interconnect trees, the average training time is around 30 seconds, and the average inference time is 0.96 seconds, indicating the efficiency of the proposed method. On the other hand, COMSOL takes a significantly longer time to solve for interconnect trees at postvoiding stress, with an average runtime of approximately 2700 seconds for our experiments. From this observation, we can infer that in the case of multisegment trees, the average speedup of *PostPINN-EM* is 87X. Thus, *PostPINN-EM* can save a considerable amount of computation time compared to COMSOL and EMspice while solving multisegment interconnect structures for the post-voiding phase. Another advantage of this method is that both the first stage analytical solution and second stage PINN depend entirely on the physical and material properties of the interconnects. This completely eliminates the training data requirement and makes our method highly generalizable. Additionally, the use of this two-stage approach allows us to calculate stress at any local position at a given aging time without solving the whole interconnect at once.

VI. Conclusion

In this work, we proposed a new approach, called *PostPINN-EM*, to solve the stress evolution in the multisegment interconnects. The new method is based on the enhanced two-stage Physics-Informed Neural Networks (PINN) framework. Instead of using supervised learning method for the first stage, which turns out to be a challenging problem for post-voiding phase, we propose to use analytic solutions to consider wires with and without voids. Numerical results on some synthesized multi-segment interconnects show that the proposed *PostPINN-EM* can achieve more than 100X speedup compared to FEM based tool COMSOL with the expense of less than 1% accuracy. Compared to state of the art tool EMspice v1.0 [1], this method can achieve more than 25X

(a) Twelve-segment tree, t=1e7 s.

(b) Twelve-segment tree, t = 1e8 s.

(c) Twelve-segment tree, t = 1e9 s.

(d) Thirty-three segment tree, t = 1e7 s.

(e) Thirty-three segment tree, t = 1e8 s.

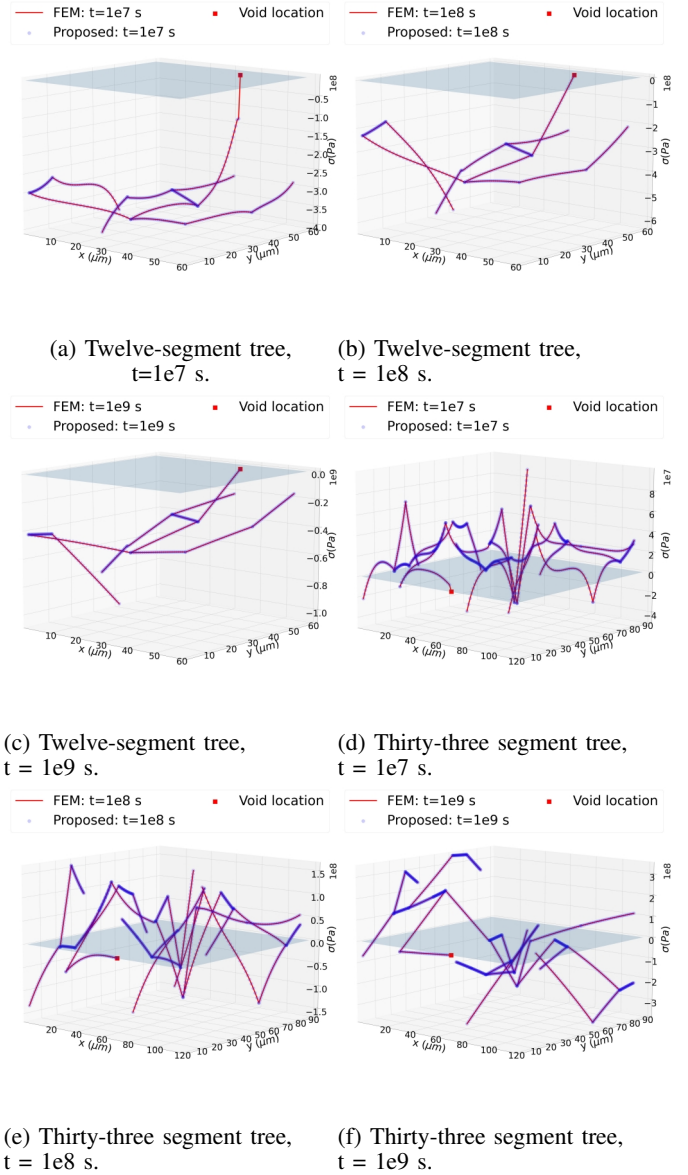(f) Thirty-three segment tree, t = 1e9 s.

Fig. 6: Comparison of the solution obtained from analytical solution with solution from FEM based COMSOL for multisegment interconnect trees. The blue plane is where $\sigma = 0$ added for readability.

speedup with similar accuracy compared to golden results from COMSOL.

References

[1] Z. Sun, S. Yu, H. Zhou, Y. Liu, and S. X.-D. Tan, "EMSpice: Physics-Based Electromigration Check Using Coupled Electronic and Stress Simulation," *IEEE Transactions on Device and Materials Reliability*, vol. 20, no. 2, pp. 376–389, Jun. 2020.

[2] J. R. Black, "Electromigration-A Brief Survey and Some Recent Results," *IEEE Trans. on Electron Devices*, vol. 16, no. 4, pp. 338–347, Apr. 1969.

[3] I. A. Blech, "Electromigration in thin aluminum films on titanium nitride," *Journal of Applied Physics*, vol. 47, no. 4, pp. 1203–1208, 1976.

[4] M. Hauschildt, C. Hennesthal, G. Talut, O. Aubel, M. Gall, K. B. Yeap, and E. Zschech, "Electromigration Early Failure Void Nucleation and Growth Phenomena in Cu And Cu(Mn) Interconnects," in *IEEE Int. Reliability Physics Symposium (IRPS)*, 2013, pp. 2C.1.1–2C.1.6.

[5] V. Sukharev, "Beyond Black's Equation: Full-Chip EM/SM Assessment in 3D IC Stack," *Microelectronic Engineering*, vol. 120, pp. 99–105, 2014.

[6] M. A. Korhonen, P. Bo/rgesen, K. N. Tu, and C.-Y. Li, "Stress evolution due to electromigration in confined metal lines," *Journal of Applied Physics*, vol. 73, no. 8, pp. 3790–3799, 1993.

[7] R. De Orio, H. Ceric, and S. Selberherr, "Physically based models of electromigration: From black's equation to modern tcad models," *Microelectronics Reliability*, vol. 50, no. 6, pp. 775–789, 2010.

[8] X. Huang, A. Kteyan, S. X.-D. Tan, and V. Sukharev, "Physics-Based Electromigration Models and Full-Chip Assessment for Power Grid Networks," *IEEE Trans. on Computer-Aided Design of Integrated Circuits and Systems*, vol. 35, no. 11, pp. 1848–1861, Nov. 2016.

[9] V. Sukharev, A. Kteyan, and X. Huang, "Postvoiding stress evolution in confined metal lines," *IEEE Transactions on Device and Materials Reliability*, vol. 16, no. 1, pp. 50–60, 2016.

[10] H. Chen, S. X.-D. Tan, X. Huang, T. Kim, and V. Sukharev, "Analytical modeling and characterization of electromigration effects for multibranch interconnect trees," *IEEE Trans. on Computer-Aided Design of Integrated Circuits and Systems*, vol. 35, no. 11, pp. 1811–1824, 2016.

[11] V. Mishra and S. S. Sapatnekar, "Predicting Electromigration Mortality Under Temperature and Product Lifetime Specifications," in *Proc. Design Automation Conf. (DAC)*. ACM/EDAC/IEEE, June 2016, pp. 1–6.

[12] H.-B. Chen, S. X.-D. Tan, J. Peng, T. Kim, and J. Chen, "Analytical modeling of electromigration failure for vlsi interconnect tree considering temperature and segment length effects," *IEEE Transaction on Device and Materials Reliability (T-DMR)*, vol. 17, no. 4, pp. 653–666, 2017.

[13] S. Chatterjee, V. Sukharev, and F. N. Najm, "Power Grid Electromigration Checking Using Physics-Based Models," *IEEE Transactions on Computer-Aided Design of Integrated Circuits and Systems*, vol. 37, no. 7, pp. 1317–1330, Jul. 2018.

[14] C. Cook, Z. Sun, E. Demircan, M. D. Shroff, and S. X.-D. Tan, "Fast electromigration stress evolution analysis for interconnect trees using krylov subspace method," *IEEE Trans. on Very Large Scale Integration (VLSI) Systems*, vol. 26, no. 5, pp. 969–980, May 2018.

[15] S. Wang, Z. Sun, Y. Cheng, S. X.-D. Tan, and M. Tahoori, "Leveraging recovery effect to reduce electromigration degradation in power/ground TSV," in *Proc. Int. Conf. on Computer Aided Design (ICCAD)*. IEEE, Nov. 2017, pp. 811–818.

[16] H. Zhao and S. X.-D. Tan, "Postvoiding fem analysis for electromigration failure characterization," *IEEE Trans. on Very Large Scale Integration (VLSI) Systems*, vol. 26, no. 11, pp. 2483–2493, Nov. 2018.

[17] A. Abbasinasab and M. Marek-Sadowska, "RAIN: A tool for reliability assessment of interconnect networks—physics to software," in *Proc. Design Automation Conf. (DAC)*. New York, NY, USA: ACM, 2018, pp. 133:1–133:6.

[18] L. Chen, S. X.-D. Tan, Z. Sun, S. Peng, M. Tang, and J. Mao, "Fast analytic electromigration analysis for general multisegment interconnect wires," *IEEE Transactions on Very Large Scale Integration (VLSI) Systems*, pp. 1–12, 2019.

[19] A. Shohel, M. Abdullah, V. A. Chhabria, N. Evmorfopoulos, and S. S. Sapatnekar, "Analytical modeling of transient electromigration stress based on boundary reflections," in *2021 IEEE/ACM International Conference On Computer Aided Design (ICCAD)*, 2021, pp. 1–8.

[20] S. X.-D. Tan, M. Tahoori, T. Kim, S. Wang, Z. Sun, and S. Kiamehr, *VLSI Systems Long-Term Reliability – Modeling, Simulation and Optimization*. Springer Publishing, 2019.

[21] S. P. Hau-Riege and C. V. Thompson, "Experimental characterization and modeling of the reliability of interconnect trees," *Journal of Applied Physics*, vol. 89, no. 1, pp. 601–609, 2001.

[22] M. Raissi, "Deep hidden physics models: Deep learning of nonlinear partial differential equations," *The Journal of Machine Learning Research*, vol. 19, no. 1, pp. 932–955, 2018.

[23] M. Raissi, P. Perdikaris, and G. E. Karniadakis, "Physics-informed neural networks: A deep learning framework for solving forward and inverse problems involving nonlinear partial differential equations," *Journal of Computational Physics*, vol. 378, pp. 686–707, 2019.

[24] T. Hou, N. Wong, Q. Chen, Z. Ji, and H.-B. Chen, "A space-time neural network for analysis of stress evolution under dc current stressing," *IEEE Transactions on Computer-Aided Design of Integrated Circuits and Systems*, pp. 1–1, 2022.

[25] W. Jin, L. Chen, S. Lamichhane, M. Kavousi, and S. X.-D. Tan, "Hierpinn-em: Fast learning-based electromigration analysis for multi-segment interconnects using hierarchical physics-informed neural network," in *Proc. Int. Conf. on Computer Aided Design (ICCAD)*, 2022, pp. 1–9.

[26] T. Hou, P. Zhen, N. Wong, Q. Chen, G. Shi, S. Wang, and H.-B. Chen, "Multilayer perceptron-based stress evolution analysis under dc current stressing for multisegment wires," *IEEE Transactions on Computer-Aided Design of Integrated Circuits and Systems*, vol. 42, no. 2, pp. 544–557, 2023.

[27] X. Wang, Y. Yan, J. He, S. X.-D. Tan, C. Cook, and S. Yang, "Fast physics-based electromigration analysis for multi-branch interconnect trees," in *Proc. Int. Conf. on Computer Aided Design (ICCAD)*. IEEE, Nov. 2017, pp. 169–176.

[28] V. Sukharev, A. Kteyan, and X. Huang, "Post-Voiding Stress Evolution in Confined Metal Lines," *IEEE Trans. on Device and Materials Reliability*, vol. 16, no. 1, pp. 50–60, 2016.

[29] X. Huang, A. Kteyan, S. X.-D. Tan, and V. Sukharev, "Physics-Based Electromigration Models and Full-Chip Assessment for Power Grid Networks," *IEEE Trans. on Computer-Aided Design of Integrated Circuits and Systems*, vol. 35, no. 11, pp. 1848–1861, 2016.

[30] C. Cook, Z. Sun, E. Demircan, M. D. Shroff, and S. X.-D. Tan, "Fast Electromigration Stress Evolution Analysis for Interconnect Trees Using Krylov Subspace Method," *IEEE Trans. on Very Large Scale Integration (VLSI) Systems*, vol. 26, no. 5, pp. 969–980, May 2018.

[31] Y. LeCun, Y. Bengio, and G. Hinton, "Deep learning," *Nature*, vol. 521, pp. 436–444, May 2015.

[32] I. Goodfellow, Y. Bengio, and A. Courville, *Deep learning*. MIT press, 2016, http://www.deeplearningbook.org.

[33] J. Tompson, K. Schlachter, P. Sprechmann, and K. Perlin, "Accelerating eulerian fluid simulation with convolutional networks," ser. Proceedings of Machine Learning Research, D. Precup and Y. W. Teh, Eds., vol. 70. International Convention Centre, Sydney, Australia: PMLR, 06–11 Aug 2017, pp. 3424–3433.

[34] W. Jin, S. Peng, and S. X.-D. Tan, "Data-driven electrostatics analysis based on physics-constrained deep learning," in *Proc. Design, Automation and Test In Europe Conf. (DATE)*, Feb. 2021, pp. 1–6.

[35] W. Jin, S. Sadiqbatcha, Z. Sun, H. Zhou, and S. X.-D. Tan, "Emgan: Data-driven fast stress analysis for multi-segment interconnects," in *Proc. IEEE Int. Conf. on Computer Design (ICCD)*, Oct. 2020, pp. 296–303.

[36] W. Jin, L. Chen, S. Sadiqbatcha, S. Peng, and S. X.-D. Tan, "Emgraph: Fast learning-based electromigration analysis for multi-segment interconnect using graph convolution networks," in *2021 58th ACM/IEEE Design Automation Conference (DAC)*, 2021, pp. 919–924.

[37] M. Raissi, P. Perdikaris, and G. E. Karniadakis, "Physics Informed Deep Learning (Part I): Data-driven Solutions of Nonlinear Partial Differential Equations," *arXiv e-prints*, p. arXiv:1711.10561, Nov. 2017.

[38] J. Sirignano and K. Spiliopoulos, "DGM: A deep learning algorithm for solving partial differential equations," *Journal of Computational Physics*, vol. 375, pp. 1339 – 1364, 2018.

[39] X. Meng and G. E. Karniadakis, "A composite neural network that learns from multi-fidelity data: Application to function approximation and inverse pde problems," *Journal of Computational Physics*, vol. 401, p. 109020, 2020.

[40] Y. Yang and P. Perdikaris, "Physics-informed deep generative models," *arXiv e-prints*, p. arXiv:1812.03511, Dec. 2018.

[41] J. Berg and K. Nyström, "A unified deep artificial neural network approach to partial differential equations in complex geometries," *Neurocomputing*, vol. 317, pp. 28 – 41, 2018.

[42] S. Choudhary, "Physics informed neural networks," Electronic Design Process Symposium Lecture, NVIDIA, 10 2019. [Online]. Available: http://edpsieee.ieeesiliconvalley.org/Papers/4-3_Sanjay_Choudhry_AI_Computational_Science%20.pdf

[43] V. Sukharev, A. Kteyan, and X. Huang, "Postvoiding stress evolution in confined metal lines," *IEEE Transactions on Device and Materials Reliability*, vol. 16, no. 1, pp. 50–60, 2016.

[44] Z. Liu, H.-B. Chen, and T. Hou, "Stress evolution analysis of em-induced void growth for multi-segment interconnect wires," in *2020 IEEE Asia Pacific Conference on Circuits and Systems (APCCAS)*, 2020, pp. 62–65.

[45] J. D. Bondurant and S. A. Fulling, "The dirichlet-to-robin transform," *Journal of Physics A: Mathematical and General*, vol. 38, no. 7, pp. 1505–1532, feb 2005. [Online]. Available: https://doi.org/10.1088%2F0305-4470%2F38%2F7%2F007